Precision Engineering 66 (2020) 315–323

Contents lists available at ScienceDirect

Precision Engineering

journal homepage: http://www.elsevier.com/locate/precision

Effect of speed on material removal behavior in scribing of monocrystalline silicon

Bing Wang *, Shreyes N. Melkote, Peizhi Wang, Swagath Saraogi

George W. Woodruff School of Mechanical Engineering, Georgia Institute of Technology, Atlanta, 30332, GA, USA

ARTICLE INFO

Keywords:
Material removal behavior
High-speed scribing
Strain rate
Monocrystalline silicon

ABSTRACT

This paper investigates the effect of scribing speed on the surface morphology and material removal behavior in diamond wire sawing of monocrystalline silicon through specially designed high-speed diamond scribing experiments. High-speed scribing tests are performed on a (100) monocrystalline silicon wafer over a wide range of speeds. The results show that a higher scribing speed is prone to inducing more surface defects such as burrs and tearing in the ductile scribing region, and more radial cracks in the brittle scribing region. The critical scribing depth of ductile-to-brittle transition is found to decrease with increasing scribing speed. A strain rate hardening effect is evident in the experimental data, which explains the underlying mechanism for promotion of brittle fracture at higher scribing speeds.

1. Introduction

Silicon is widely used in a number of fields such as optics, photovoltaics, and microelectronics. Because of its higher productivity, diamond wire sawing (DWS) is normally preferred over loose abrasive slurry sawing for the manufacture of silicon wafers [1–3]. Production of silicon wafers with low surface damage is a challenge due to the inherent brittleness of silicon. Previous research has shown that deformation below a threshold can lead to ductile deformation instead of the normally expected brittle fracture [4–6]. The factors that determine the deformation mode (i.e. ductile or brittle fracture) of silicon in DWS include the shape of abrasives used [7], the cutting environment (i.e. dry or with coolant) [8], and the sawing parameters [9,10].

Compared to other influencing factors, there is limited fundamental understanding of the effect of scribing speed, which is a key process parameter in DWS, on the deformation mode and material removal behavior of silicon. Considering that DWS is characterized by a combination of indentation and scratching processes, prior research has focused on nanoindentation and scribing of silicon to investigate the material deformation behavior and the underlying mechanisms [11–13]. However, most of the available literatures on scribing/-scratching of monocrystalline silicon are limited to low speeds (10 μm/s – 2.67 mm/s), compared to the high speeds (10 m/s – 20 m/s) routinely used in DWS of silicon wafers [8,11–13]. Therefore, there is a large gap in fundamental understanding of the deformation behavior of silicon at scribing speeds representative of the DWS process.

Several researchers [14–16] have tried high-speed scribing experiments on monocrystalline silicon. Wegener et al. [14] used a wire wrapped grinding wheel to perform high-speed scribing experiments on bulk silicon at a scribing speed of 50 m/s. Their objective was to study the wear behavior of diamond wires at high speeds and no results on the deformation behavior of silicon as a function of scribing speed were reported. Alreja and Subbiah [15] used a specialized setup to perform scribing tests at a fixed speed of 1 m/s on (100) monocrystalline silicon wafer, and they detected more metastable silicon phases such as Si-III, Si-XII, Si-IV, and Si-XIII along with amorphous silicon (a-Si) within the scribes. Zhang et al. [16] used grinding with diamond tips to conduct high-speed scribing tests at a fixed speed of 40 m/s on a (100) monocrystalline silicon wafer. They found that complete amorphization occurred underneath the scriber tip. It can be seen that the speeds used in the above studies were either significantly lower or higher than the speeds used in DWS. In addition, the scribing speed in these studies was kept constant and hence the effect of scribing speed on material deformation was not revealed.

The effect of scribing speed, and the corresponding strain rate, on the mechanical properties of silicon determines the material deformation behavior in the DWS process. An appropriate material model considering the strain rate effect is required for accurate prediction of dynamic deformation and fracture when using numerical methods such as the finite element method (FEM). However, most of the current FEM models

* Corresponding author.
E-mail address: bwang427@gatech.edu (B. Wang).

https://doi.org/10.1016/j.precisioneng.2020.07.011
Received 15 December 2019; Received in revised form 17 July 2020; Accepted 27 July 2020
Available online 3 August 2020
0141-6359/© 2020 Elsevier Inc. All rights reserved.

of silicon scribing utilize a static or quasi-static material model [12,17,18]. Unlike metallic materials, it is difficult to employ dynamic material testing methods such as the Split Hopkinson pressure bar (SHPB) technique to understand and quantify the dynamic deformation behavior of silicon, primarily due to its brittleness. As a result, it is necessary to develop a material model of silicon considering the strain rate effect, especially one that is representative of strain rates encountered in DWS.

This paper investigates the effect of scribing speed and the corresponding strain rate on the deformation and surface damage behavior of monocrystalline silicon using a specialized high-speed scribing setup. The ductile deformation, brittle fracture, as well as ductile-to-brittle transition of silicon over a wide range of scribing speeds (1.67×10^{-5} m/s – 25 m/s) are studied. The average stresses beneath the scriber at different scribing speeds are analyzed to reveal the underlying mechanisms of material removal. A quantitative relationship between the average normal and tangential stress and strain rate is developed, which suggests a strain rate dependence of the plastic deformation of monocrystalline silicon.

2. Experimental procedure

The experimental setup for high-speed scribing of silicon is shown in Fig. 1. Microelectronic grade polished monocrystalline (100) silicon wafers were used in the scribing experiments. Conical tipped diamond scribers with 120° included angle and a tip radius of 3 μm were used. The silicon wafer, with a diameter of 101.6 mm, was sliced into 10 mm × 25 mm coupons, which were attached to a vacuum chuck bolted on to a three-component piezoelectric force dynamometer (Kistler 9256c2). The dynamometer was used to detect contact between the diamond scriber and the silicon coupon, and to measure the scribing forces in three orthogonal directions. The dynamometer was mounted on X-Y-Z motion stages (Aerotech ANT-4V), which had a positioning resolution of 1 nm in the scribing depth (Z) direction. High scribing speeds were realized by means of a high-speed motor spindle (Fraureuth FS 33–60) with a speed range of 5000–60,000 RPM. The diamond scriber was fixed to an aluminum cutting disk [Fig. 1(b)] at a radius of 19 mm. The cutting disk was attached to the high-speed spindle.

All scribing experiments at speeds ranging from 10 m/s to 25 m/s were conducted using the high-speed rotation of the spindle. The scribing direction is shown schematically in Fig. 1(c). The region of the scribes selected for subsequent observation and analysis is located in the middle of the silicon coupon where the scribing direction is [110]. The low speed scribing experiments over the 1 mm/min – 10,000 mm/min range were performed using the linear movement of the X–Y motion stages with the diamond scriber mounted in the spindle, which was locked and therefore not rotating. The scribing direction in the low speed experiments was also [110]. In both sets of experiments, two constant scribing depths of 200 nm and 500 nm were used to investigate the ductile deformation and brittle fracture of silicon, respectively.

Furthermore, inclined scribing experiments were performed at both the high speed and low speed ranges to study the ductile-to-brittle transition of silicon. A thin shim was placed under one side of the silicon coupon to create a scribing depth variation from 0 to 3 μm over a 10 mm length along the scribing direction (i.e. an inclined surface is formed with a computed slope of 0.03°). The location of the shim is marked in Fig. 1(d). Although there was a small clearance between the bottom

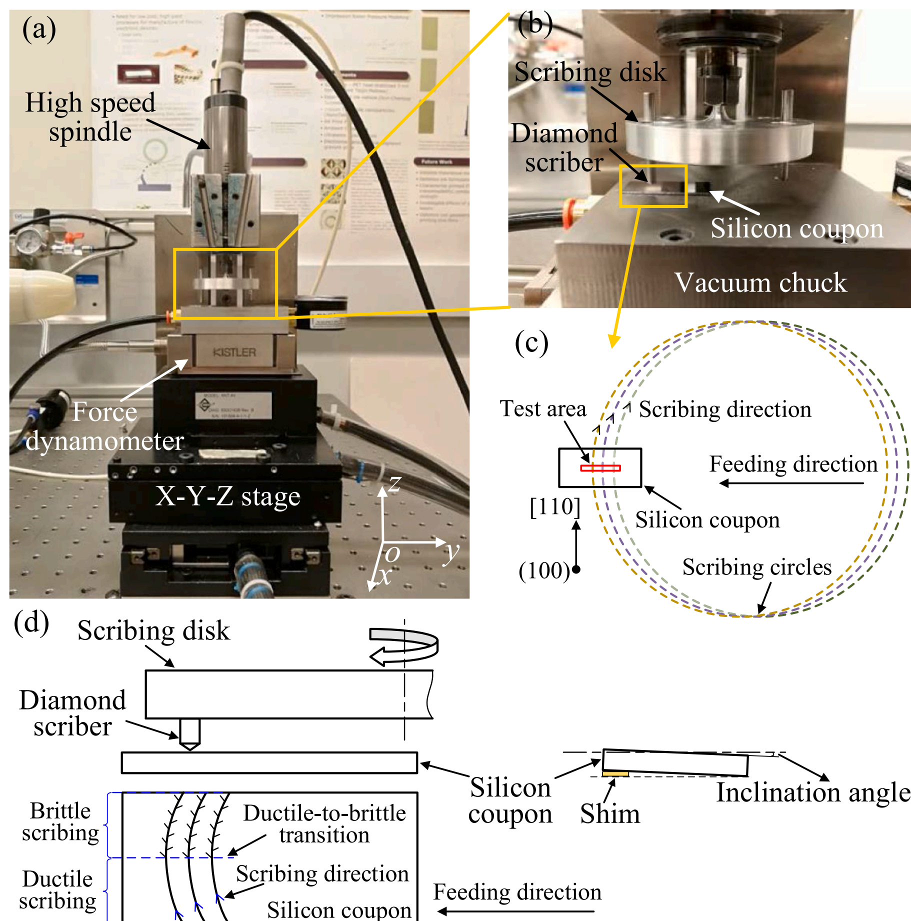

Fig. 1. Experimental setup for high-speed scribing (a) overall setup, (b) scribing disk, (c) schematic of scribing test, and (d) three-view schematic of inclined scribing. Note: the dimensions of the scribing disk, diamond scriber, and silicon coupon are not to scale. (For interpretation of the references to colour in this figure legend, the reader is referred to the Web version of this article.)

surface of the silicon coupon and the vacuum chuck, the silicon coupon was still firmly fixed to the chuck because the inclination angle was only 0.03°. The critical depths of ductile-to-brittle transition for all the scribing speeds investigated were then obtained from the inclined scribing tests. It should be noted that the scribing direction at the location of the ductile-to-brittle transition in the 10 m/s – 25 m/s range may not be strictly parallel with [110]. Nevertheless, the variation of scribing direction was determined to be less than 3°in the ductile-to-brittle transition region. The effect of this small variation on the scribing direction is assumed to be negligible.

The experimental design employed for the two sets of scribing tests is presented in Table 1. The tests for each scribing condition were repeated five times on one coupon (i.e. five scribes per scribing speed were made) for speeds ranging from 1 mm/min to 10,000 mm/min. Over ten scribes were made on one coupon at each scribing speed ranging from 10 m/s to 25 m/s, and five of them per scribing speed were randomly selected for analysis.

Micro-Raman spectroscopy was performed on selected scribes using a Raman spectrometer (Renishaw Invia) to detect the phases produced in the scribed grooves. An argon ion laser with a wavelength of 488 nm and a beam size of 1 μm was used. The residual depths and surface radial crack frequencies of the scribed grooves were measured using a 3D optical profiler (Zygo ZeGage, 50X objective). High resolution images of the scribed grooves were obtained using a scanning electron microscope (Zeiss Ultra60).

3. Results and discussion

3.1. Surface morphology of scribed grooves

Fig. 2 shows the surface morphologies of the scribed grooves produced at scribing speeds varying from 1 mm/min to 25 m/s and a constant scribing depth of 200 nm. No brittle fracture features were observed in the scribed grooves or near the groove edges as shown in Fig. 2, which indicates that all grooves were produced in the ductile deformation mode. Both continuous and fragmented chips were observed near the edges of all scribed grooves. Typical SEM images of the chips produced at different scribing speeds are shown in Fig. 3.

The groove morphologies generated at different scribing speeds exhibit some differences. The 1 mm/min scribed groove [Fig. 2(a)] was much smoother than those generated at higher scribing speeds. When the scribing speed was higher than 10 mm/min, different defects occurred within the grooves as shown in Fig. 2(b)–(i). The defects include burrs, tearing, periodic ductile cracking and debris depending on the scribing speed. The burr type morphologies observed at the scribing speed of 10 mm/min are similar with those seen at 100 mm/min. When the scribing speed is increased to 1000 mm/min and to 10,000 mm/min, tearing accompanied by burrs within the scribed grooves, and periodic ductile cracking were observed, respectively. Features similar to periodic cracks shown in Fig. 2(e) were also observed in the scribes made on a multi-crystalline silicon surface using an actual diamond wire [19]. With increase in the scribing speed to 10 m/s – 25 m/s, the main surface features within the scribed grooves are primarily debris.

A possible reason for the formation of surface defects is the micro-geometry of the imperfect diamond scriber tip. Specifically, protrusions or pits on the scriber tip, as seen in Fig. 4, may cause heterogeneous plastic deformation of silicon, which causes the above-mentioned defects. However, this reason cannot explain the propensity for such defects at higher scribing speeds. These defects are more likely caused by the varied mechanical loading between the scriber tip and the deformed material at different scribing speeds, which will be discussed later. Furthermore, the formation of debris at scribing speeds higher than 10 m/s is probably due to the generation of more fragmented chips at the higher speeds. These results suggest that lower speeds are beneficial for improving the cut surface quality during scribing of silicon. However, such low speeds are impractical in DWS of silicon.

Table 1
Experimental design.

Experiments	Scribing speed	Scribing depth	Remarks
1	1 mm/min – 10,000 mm/min, 10 m/s – 25 m/s	200 nm and 500 nm	Constant scribing depths were used without shim
2	1 mm/min – 10,000 mm/min, 10 m/s – 25 m/s	Varied scribing depth	Inclined scribing experiments were performed with a thin shim under the coupon

Phase transformation beneath the scriber is responsible for the ductile removal of silicon. Micro-Raman spectroscopy was performed on selected scribes to investigate the phase transformations of silicon. Fig. 5 shows the Raman spectra of two representative tested positions within the scribed grooves labeled as A and B in Fig. 2(a) and (f), respectively. It can be seen in Fig. 5(a) that Si-III, Si-IV, Si-XII, and amorphous (a-Si) phases of silicon are formed in the 1 mm/min scribed groove, whereas only Si-IV and a-Si are found in the 10 m/s scribed groove as seen in Fig. 5(b). The latter observation is attributed to the high unloading rate associated with the high scribing speed of 10 m/s, which results in complete amorphization within the scribed groove. It is worth noting that Si-III, Si-XII, and a-Si occur in ductile scribing regions of the silicon wafer, which indicates that the formation of such phases implies the ductile deformation of silicon [20–22]. Furthermore, Si-IV with high intensity count was detected in both scribes made at 1 mm/min and 10 m/s. It is known that the formation mechanism of Si-IV is due to the intersection of twins produced by the plastic deformation of Si-I [23,24]. Additional results for the effect of scratching speed on phase transformations in high-speed scribing of monocrystalline silicon are available in Ref. [25].

It should be noted that test position B in Fig. 2(f) may partially cover the groove and debris. It is difficult to perform micro-Raman tests on the groove surface without interference of debris due to limitation of the laser beam size (1 μm) and large amounts of debris formed within the groove at high scribing speeds. Nevertheless, multiple measurements at different locations within the scribed grooves were made, and the results were reasonably consistent. Therefore, it can be assumed that the interference of debris does not significantly influence the phase measurement of the groove surface at the investigated location using the scribing parameters in Fig. 2(f), where only ductile scribing occurs.

Fig. 6 shows the SEM morphologies of scribed grooves made at scribing speeds ranging from 1 mm/min to 25 m/s at a scribing depth of 500 nm. Chevron cracks are observed near the edges of all scribed grooves, indicating brittle regime scribing occurred at the 500 nm scribing depth over the entire range of scribing speeds investigated. Chipping caused by brittle fracture is also found to occur near the groove edges as seen in Fig. 6(d) and (e). With increasing scribing speed, the space between adjacent radial cracks tends to decrease, leading to a higher frequency of radial crack formation. Meanwhile, the crack length was also larger at higher scribing speeds due to either a higher loading stress or material embrittlement induced by higher loading and unloading rates.

Chevron cracks were prone to occur on one side of the grooves as shown in Fig. 6, indicating in-plane anisotropy of material deformation and fracture during scribing of monocrystalline silicon [20,26]. One possible reason for this phenomenon is that the applied stress distribution in the two sides of the scribed groove may not be uniform or symmetric due to imperfections in the micro-geometry of the diamond scriber tips used in the experiments (as seen in Fig. 4). The groove side with higher stress would therefore fracture more easily. Once cracks were formed on one side of the scribed groove, the stress applied on the silicon wafer would be relieved, after which the other side of the groove would not fracture easily.

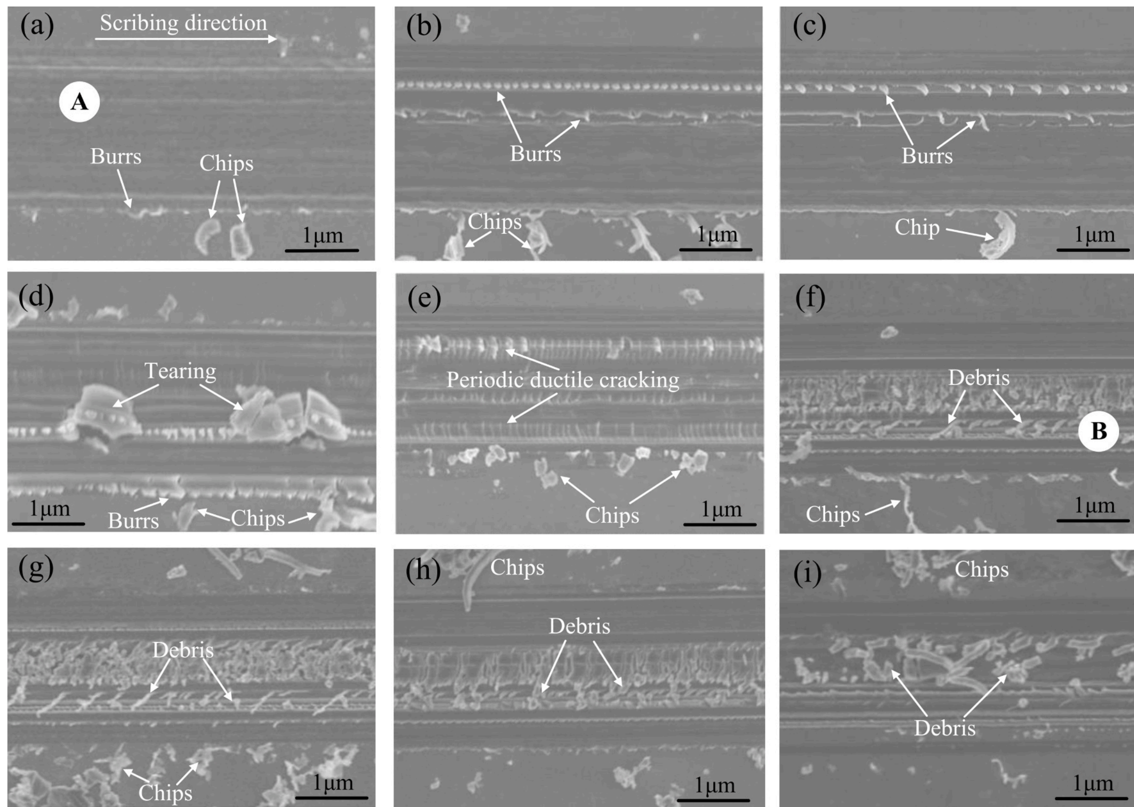

Fig. 2. Surface morphologies of scribed grooves made at a scribing depth of 200 nm at different speeds (a) 1 mm/min, (b) 10 mm/min, (c) 100 mm/min, (d) 1000 mm/min, (e) 10,000 mm/min, (f) 10 m/s, (g) 15 m/s, (h) 20 m/s, and (i) 25 m/s.

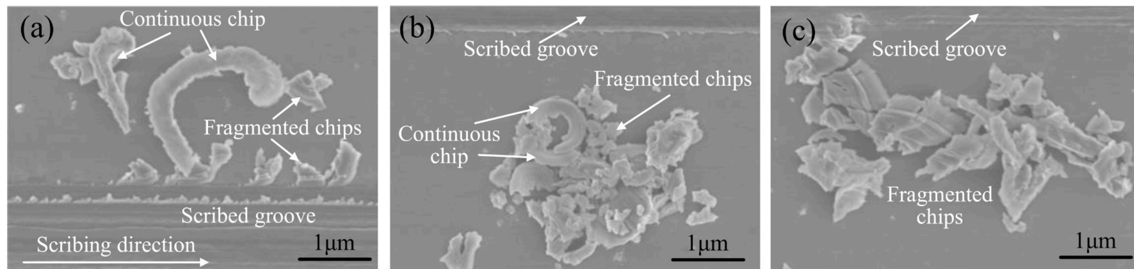

Fig. 3. Chip morphologies produced at a scribing depth of 200 nm at different speeds (a) 1 mm/min, (b) 1000 mm/min, and (c) 20 m/s.

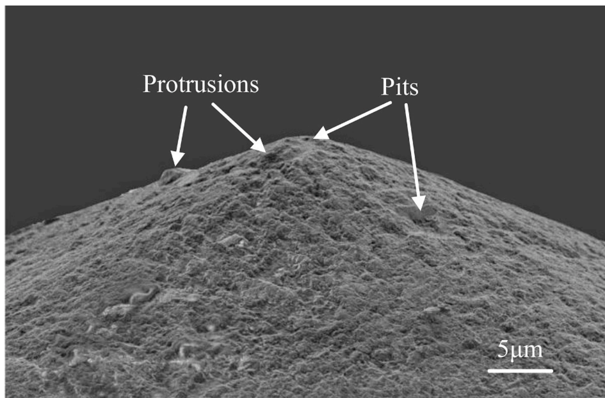

Fig. 4. SEM morphology of a diamond tip used in the scribing tests.

It must be noted that the use of two different methods to produce relative motion between the scriber and silicon coupon (linear motion and spindle rotation) can influence the experimental results. Therefore, a high speed camera (Phantom VEO 410L) was used to observe the instantaneous motion of the scriber during scribing and no significant differences were observed between the two scribing methods. Furthermore, no evidence of vibration was visible in the scribed morphologies, as seen in Figs. 2 and 6. As a result, it is deemed that the scribing method did not significantly influence the experimental results.

The frequency of radial cracks formed at different scribing speeds was analyzed quantitatively as shown in Fig. 7. The counts of radial cracks per millimeter derived from analysis of data obtained from an optical profiler (Zygo ZeGage, 50× objective) was used to quantify the radial crack frequency. Two representative optical images of the scribed grooves created at 100 mm/min and 10 m/s were inserted in Fig. 7. It can be seen from the figure that the frequency of radial cracks is linearly correlated with the logarithm of scribing speed. When the scribing speed is greater than 10 m/s, the frequency of radial cracks tends to saturate at ~150 mm^{-1}. The recent work of Trachet and Subhash [27] on nano-indentation of (100) monocrystalline silicon also reported that cracking

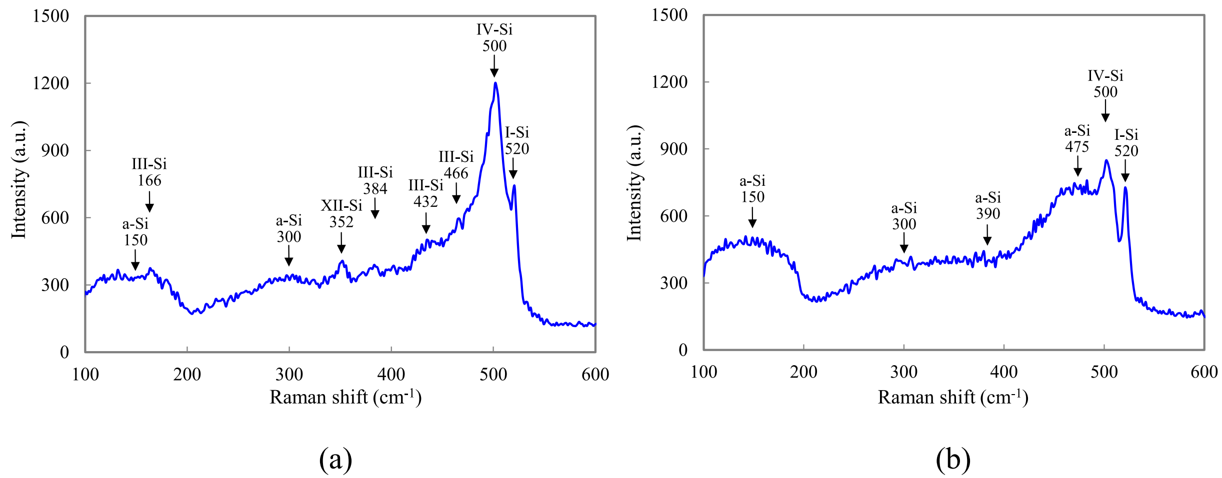

Fig. 5. Raman spectra of tested positions within scribed grooves made at different speeds (a) Position A in Fig. 2(a) made at 1 mm/min, (b) Position B in Fig. 2(f) made at 10 m/s.

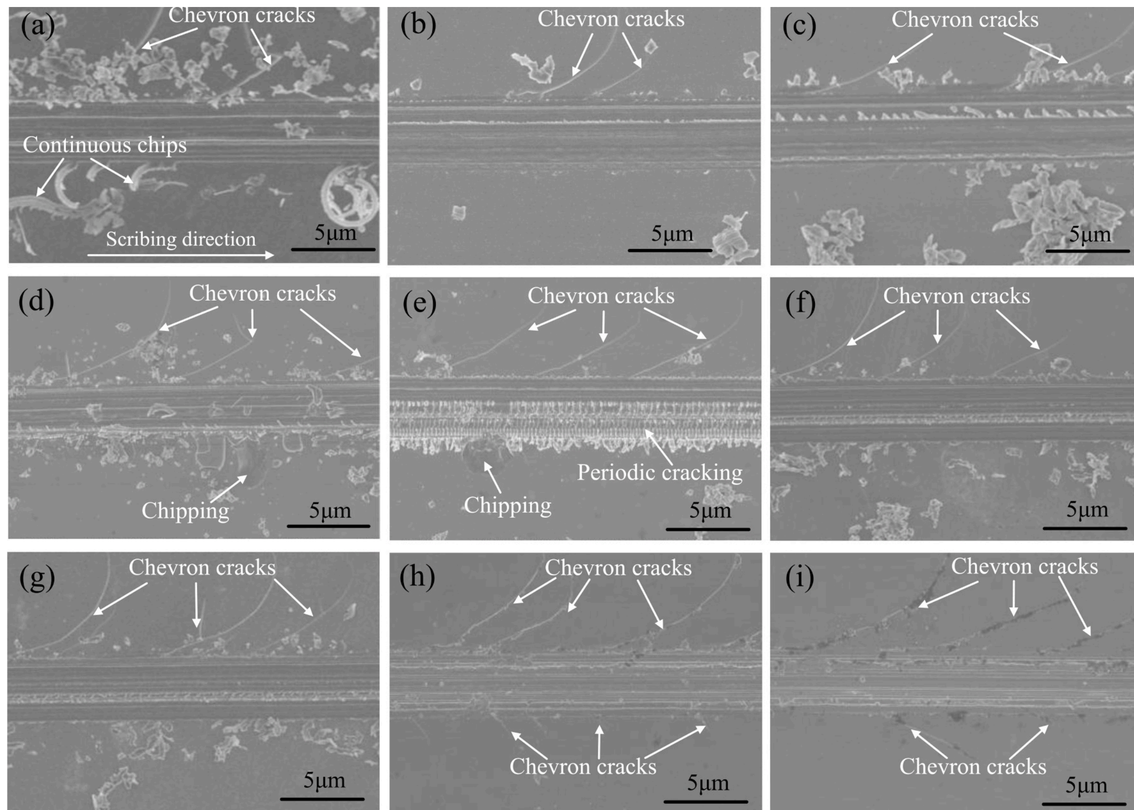

Fig. 6. SEM morphologies of scribed grooves made at a scribing depth of 500 nm under different speeds (a) 1 mm/min, (b) 10 mm/min, (c) 100 mm/min, (d) 1000 mm/min, (e) 10,000 mm/min, (f) 10 m/s, (g) 15 m/s, (h) 20 m/s, and (i) 25 m/s.

was generally more severe in dynamic indentation (loading and unloading rates of 10^2–10^4/s) compared to static indentation (loading and unloading rate of 1/s) for similar indentation loads. They attributed this finding to a lower response time for dislocation motion during dynamic indentations, which results in the more brittle behavior.

3.2. *Critical residual depth of ductile-to-brittle transition at different scribing speeds*

A critical residual depth d_c parameter for ductile-to-brittle transition was adopted to quantitatively compare the material deformation behaviors at different scribing speeds. The critical depth was defined as the residual scribing depth at the location along the scribe where the first crack on the wafer surface is observed. Fig. 8 shows a sample image of the 1 mm/min scribed groove and the procedure used to determine the critical depth parameter. It can be seen from Fig. 8(b) that bumps are formed at the groove edges due to plastic deformation of silicon. The residual depth was defined as the distance between the groove bottom and the undisturbed silicon surface.

The variation of critical residual depth of ductile-to-brittle transition with scribing speed is plotted in Fig. 9. A larger critical residual depth implies enhanced ductility of the deformed material. Fig. 9 indicates

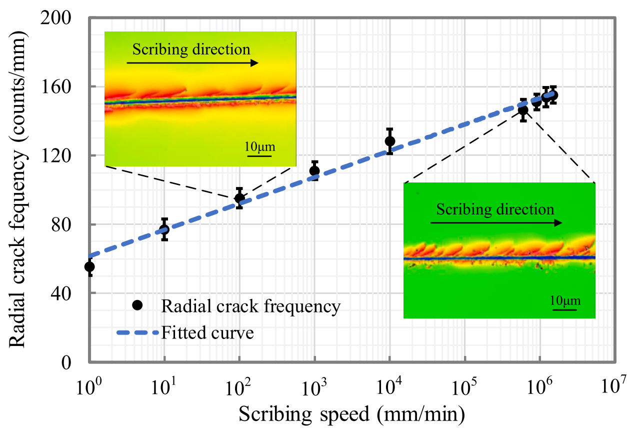

Fig. 7. Variation of radial crack frequency with scribing speed (the error bars indicate standard deviations obtained from five repeated measurements).

that the critical residual depth decreases with increasing scribing speed, indicating that brittle fracture occurs at a smaller scribing depth at higher scribing speeds. The critical residual depth parameter exhibits a negative linear correlation with the logarithm of scribing speed within the investigated speed range. When increasing the scribing speed from 1 mm/min to 25 m/s, the average critical residual depth decreases by about 40% from 264 nm to 158 nm.

3.3. Variation of scribing forces at different scribing speeds

The fluctuation of scribing forces with increasing scribing depth reflects the transition in material removal mode. Fig. 10 shows the instantaneous scribing forces, including the tangential force (F_x), the radial force (F_y) and the normal force (F_z), plotted against scribing distance. The scribing distance has a proportional relationship with the scribing depth. Hence, the tangential force F_x and the normal force F_z exhibit an increasing trend with scribing distance, while the radial force F_y remains at nearly zero due to the axisymmetric scriber used. Considering the limited bandwidth of the piezoelectric force dynamometer (<5 kHz), only the scribing forces in the 1 mm/min – 1000 mm/min range were measured and studied.

The initial smooth increase in the forces indicates ductile scribing. The transition from ductile to brittle scribing is marked by a drastic variation in the forces [8], as seen in Fig. 10. In the scribing force curves in Fig. 10, the standard deviations of scribing force component F_z (i.e. the largest force component) were calculated over consecutive scribing distances of 0.1 mm, i.e. from 0 to 0.1 mm, 0.1 mm–0.2 mm, 0.2 mm–0.3 mm, etc. It is found that beyond a standard deviation of 10% the variation in the force signal increases rapidly. Therefore, the location where the standard deviation of the force signal is greater than 10% is taken to be the ductile-to-brittle transition point. As the rate of increase of scribing depth is the same for all cases investigated, scribing at a higher speed results in the onset of brittle scribing at a shorter scribing distance, and hence at a smaller scribing depth. The scribing distances at the location of ductile-to-brittle transition were 1.50 mm, 1.30 mm, 1.10 mm and 1.10 mm corresponding to scribing speeds of 1 mm/min, 10 mm/min, 100 mm/min and 1000 mm/min, respectively.

The effect of scribing speed, which determines the strain rate, on the mechanical properties of monocrystalline silicon can be revealed by analyzing the variation of the scribing forces with scribing speed. The normal scribing force (F_z) makes the largest contribution to the hydrostatic pressure within the scribed region, and therefore is the most important force component for determining the material deformation mode i.e., ductile or brittle. The average normal stress is calculated as the ratio of the normal force to the x-y projection of the actual contact area between the scriber tip and the silicon wafer. The average tangential stress is calculated as the ratio of the tangential force to the y-z projection of the actual contact area between the scriber tip and the silicon wafer. Fig. 11 shows a three-view schematic of the contact area between the scriber and silicon wafer during the scribing test. The effect of elastic recovery on the contact area at a given scribing distance is assumed to be independent of the scribing speed over the 1 mm/min – 1000 mm/min range.

The average strain rate $\dot{\varepsilon}$ during ductile scribing is estimated as follows [28–30].

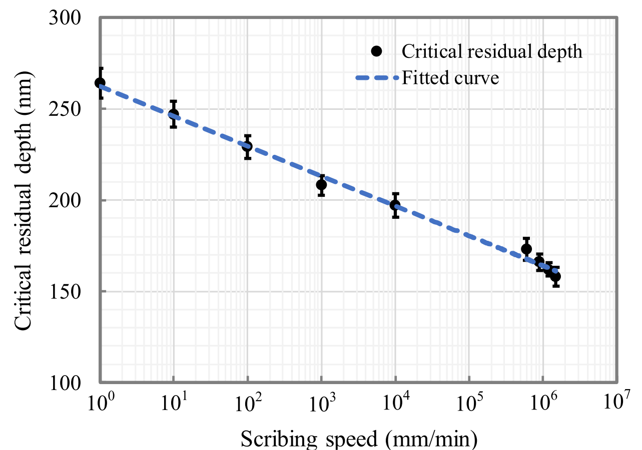

Fig. 9. Variation of critical residual depth with scribing speed (the error bars indicate standard deviations obtained from five repeated measurements).

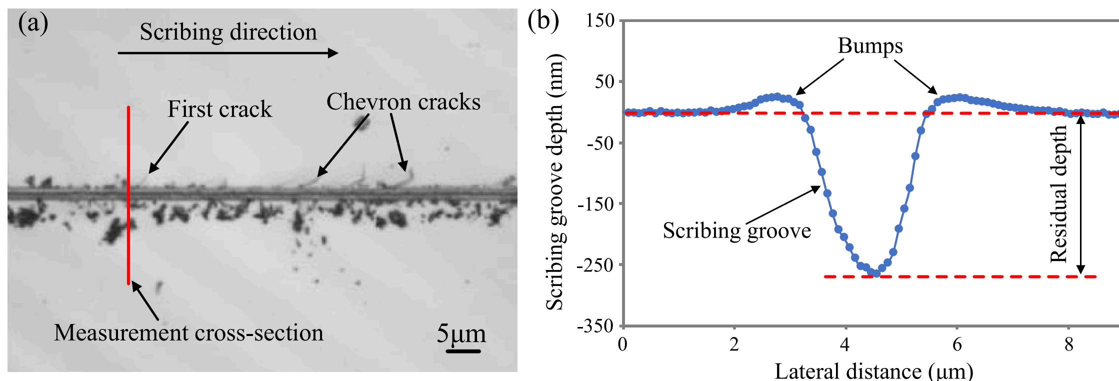

Fig. 8. Measurement of critical residual depth of ductile-to-brittle transition (a) surface morphology measured with optical profiler, (b) determination of residual scribing depth.

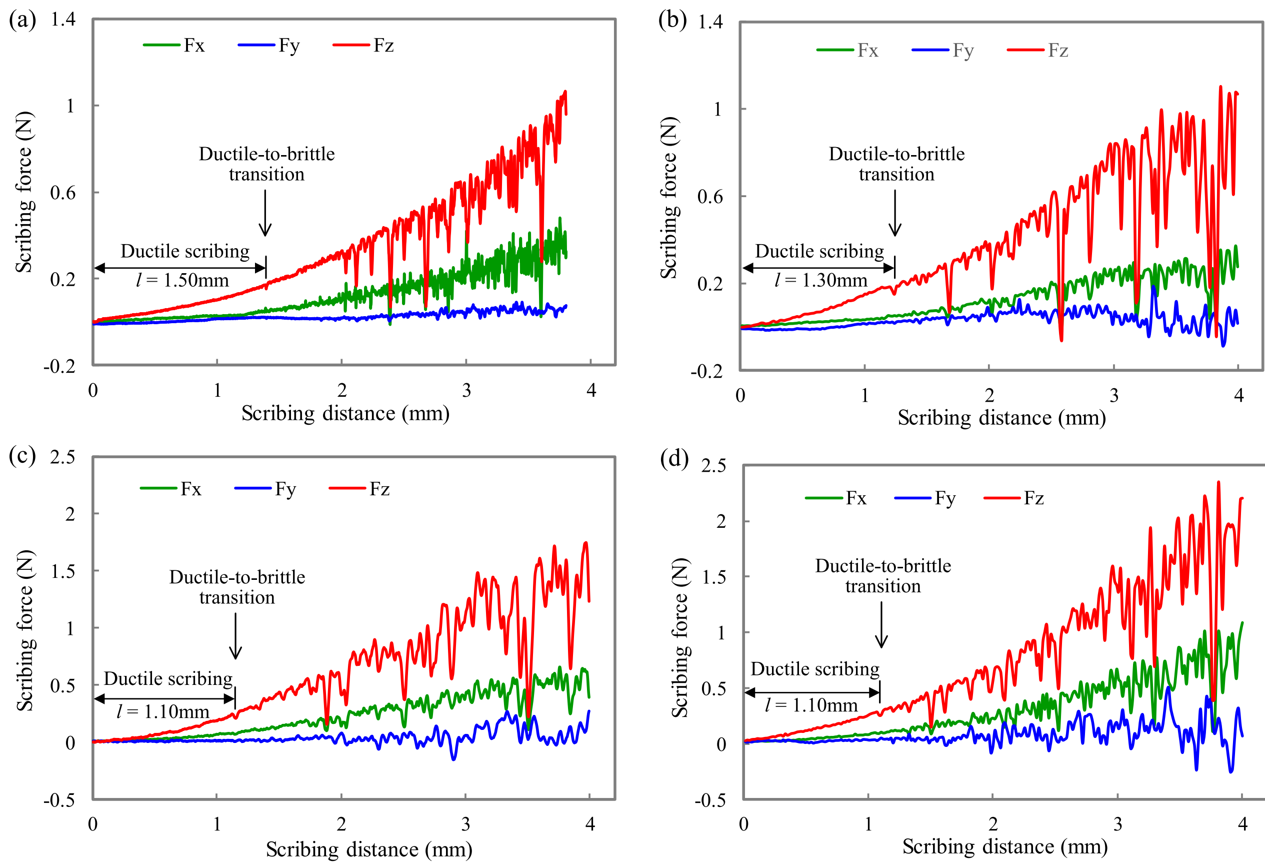

Fig. 10. Scribing force curves at different scribing speeds (a) 1 mm/min, (b) 10 mm/min, (c) 100 mm/min, and (d) 1000 mm/min. The scribing distances at which ductile-to-brittle transition occur are indicated.

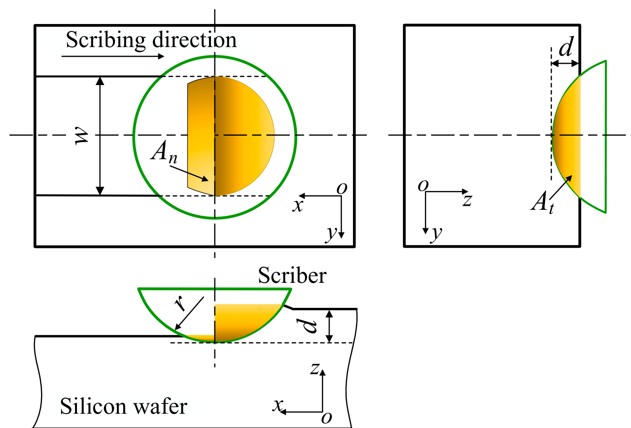

Fig. 11. Schematic of contact area between the scriber and silicon wafer during scribing test (A_n, A_t, w, d, and r denote the normal contact area, tangential contact area, scribing width, scribing depth and radius of scriber, respectively). Note: the trapezoidal shaded region in the upper left figure indicates the contact area caused by elastic recovery. (For interpretation of the references to colour in this figure legend, the reader is referred to the Web version of this article.)

$$\dot{\varepsilon} = \frac{v}{w} \tag{1}$$

where v is the scribing speed and w is the scribing width.

The average normal stress σ_z and average tangential stress σ_x during ductile scribing are calculated from Eq. (2) and Eq. (3), respectively

$$\sigma_z = \frac{F_z}{A_n} \tag{2}$$

$$\sigma_x = \frac{F_x}{A_t} \tag{3}$$

where A_n and A_t are the x-y projection and y-z projection of the actual contact area between the scriber and the silicon wafer, respectively.

By comparing the normal and tangential stresses at the same scribing depth (i.e., the same scribing distance) at different speeds, the effect of strain rate on the normal and tangential stresses is revealed and suggests a strain rate dependence of the plastic deformation of monocrystalline silicon. The strain rates and stresses are normalized by their values at 1 mm/min to simplify the analyses. The strain rates, normal scribing forces, tangential scribing forces, as well as their normalized values at scribing distances of 0.25 mm, 0.5 mm, 0.75 mm and 1.0 mm are summarized in Table 2. Note that only ductile scribing occurs at these scribing distances in the 1 mm/min – 1000 mm/min range, as indicated by the scribing force curves in Fig. 10. Both the normalized normal stress and tangential stress exhibit an increasing trend with strain rate at all investigated scribing depths.

The variation of normalized normal and tangential stresses with normalized strain rate is plotted in Fig. 12. The rate dependence of the normalized stress is found to fit well ($R^2 = 98.1\%$ and 96.4% for normal stress and tangential stress, respectively) by Eq. (4), which is similar in form to the rate dependence term in some material models [31,32].

$$\sigma = \sigma_0 \left(1 + C \cdot \ln\frac{\dot{\varepsilon}}{\dot{\varepsilon}_0}\right) \tag{4}$$

where the coefficient C is fitted to be 0.196 and 0.217 for normal stress

Table 2
Strain rate, scribing force, and normalized stress at different scribing speeds.

Scribing distance l (mm)	Scribing speed (mm/min)	Strain rate (/s)	Normalized strain rate	Scribing force (N)		Normalized stress	
				Normal force F_z	Tangential force F_x	Normal stress	Tangential stress
0.25	1	12.53	1	0.021	0.011	1	1
	10	125.31	10	0.028	0.015	1.333	1.364
	100	1.25×10^3	10^2	0.040	0.023	1.905	2.091
	1000	1.25×10^4	10^3	0.051	0.029	2.429	2.636
0.5	1	8.91	1	0.044	0.013	1	1
	10	89.12	10	0.058	0.018	1.318	1.385
	100	8.91×10^2	10^2	0.081	0.024	1.841	1.846
	1000	8.91×10^3	10^3	0.109	0.032	2.477	2.462
0.75	1	7.31	1	0.070	0.021	1	1
	10	73.10	10	0.092	0.026	1.314	1.238
	100	7.31×10^2	10^2	0.129	0.038	1.843	1.810
	1000	7.31×10^3	10^3	0.169	0.053	2.414	2.524
1.0	1	6.36	1	0.104	0.029	1	1
	10	63.61	10	0.147	0.041	1.413	1.414
	100	6.36×10^2	10^2	0.192	0.054	1.846	1.862
	1000	6.36×10^3	10^3	0.246	0.072	2.365	2.483

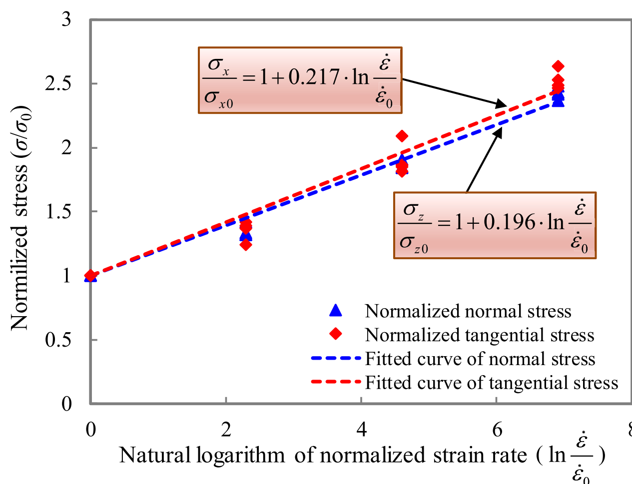

Fig. 12. Variation of normalized normal and tangential stress with normalized strain rate.

and tangential stress, respectively, in the current experiments. σ_0 and $\dot{\varepsilon}_0$ are the stress and strain rate at 1 mm/min, respectively. It indicates that the coefficient C for normal stress and tangential stress differ slightly with each other.

The rate-dependent relationship given by Eq. (4) indicates a rate hardening effect during ductile scribing of silicon, which has not been reported before. It is well known that the diamond cubic phase of crystalline silicon (Si-I) transforms to a metastable metallic phase (Si-II) with β-tin structure at a hydrostatic pressure of ~12 GPa due to the loading applied during scribing [33]. The rate hardening effect of silicon suggests that the deformation behavior of Si-II phase is sensitive to scribing speed. Generally, the phase transformation behavior of silicon is studied using a diamond anvil cell [33], wherein the loading is static or quasi-static. However, it is difficult to capture the plastic deformation behavior of the metastable Si-II phase in-situ during scribing using currently available measurement and characterization methods, mainly due to the nanometer scale deformation involved. Nevertheless, based on post-mortem examination using micro-Raman spectroscopy and the rate-dependent relationship for the stress behavior of monocrystalline silicon as shown in Fig. 12, it is plausible to infer that a strain rate hardening effect of metastable Si-II phase occurs.

Due to the strain rate hardening effect, the contact stress between the scriber and plastic deformed silicon is increased with scribing speed. Meanwhile, more radial cracks and a larger radial crack frequency occur at a higher scribing speed as seen in Figs. 6 and 7. Consequently, a relationship between the scribing speed, the contact stress and the crack formation can be established. This explains the underlying mechanism for the smaller critical depths of ductile-to-brittle transition observed at the higher scribing speeds. Furthermore, the results indicate that higher scribing speeds may lead to an increased propensity for crack formation during DWS of monocrystalline silicon, although this will also correspond to a higher material removal rate. It is therefore suggested that a balanced approach should be taken in selecting the scribing speed to optimize the material removal rate while ensuring adequate surface quality.

4. Conclusions

The paper investigated the effect of scribing speed on the material removal behavior in high-speed scribing of (100) monocrystalline silicon. Scribing tests were performed over a wide range of speeds, from 1 mm/min to 25 m/s, using a specialized high-speed scribing setup. The effects of scribing speed on the deformation behavior and ductile-to-brittle transition of monocrystalline silicon were analyzed. A higher scribing speed was found to induce more surface defects in the ductile scribing region and a larger radial crack frequency in the brittle scribing region of the scribes. An increase in scribing speed led to a reduction in the critical depth of ductile-to-brittle transition, which implied an increased tendency of material embrittlement at higher speeds.

The scribing forces under varied speeds revealed the strain rate hardening effect of monocrystalline silicon. A rate-dependent relationship for the normal and tangential stress behavior of monocrystalline silicon was derived empirically. The rate dependence of the normal stress and tangential stress explains the earlier onset of brittle scribing at higher speeds. The work described in this paper also suggests the possibility of using high speed scribing as an experimental technique to determine the dynamic mechanical properties of the material. The research presented in this paper contributes to advancing the fundamental understanding of material removal behavior of monocrystalline silicon, which is expected to be useful for the design and control of DWS of silicon wafers.

Declaration of competing interest

The authors declare that they have no known competing financial interests or personal relationships that could have appeared to influence the work reported in this paper.

Acknowledgements

The authors acknowledge the support of the National Science Foundation (CMMI Grant No.1538293) for funding the study. Parts of the work reported in the paper were performed at the Georgia Tech Institute for Electronics and Nanotechnology, a member of the National Nanotechnology Coordinated Infrastructure, which is supported by the National Science Foundation (Grant No. ECCS-1542174). The first author would also like to acknowledge the support of the International Postdoctoral Exchange Fellowship Program of China (20180064).

Appendix A. Supplementary data

Supplementary data to this article can be found online at https://doi.org/10.1016/j.precisioneng.2020.07.011.

References

[1] Wu H. Wire sawing technology: a state-of-the-art review. Precis Eng 2016;43:1–9.
[2] Kumar A, Melkote SN. Diamond wire sawing of solar silicon wafers: a sustainable manufacturing alternative to loose abrasive slurry sawing. Procedia Manuf 2018; 21:549–66.
[3] Suzuki T, Nishino Y, Yan J. Mechanisms of material removal and subsurface damage in fixed-abrasive diamond wire slicing of single-crystalline silicon. Precis Eng 2017;50:32–43.
[4] Tanaka H, Shimada S. Damage-free machining of monocrystalline silicon carbide. CIRP Annals 2013;62:55–8.
[5] Choi D-H, Lee J-R, Kang N-R, Je T-J, Kim J-Y, Jeon E-C. Study on ductile mode machining of single-crystal silicon by mechanical machining. Int J Mach Tool Manufact 2017;113:1–9.
[6] Oliaei SNB, Karpat Y. Polycrystalline diamond end mill cutting edge design to improve ductile-mode machining of silicon. Precis Eng 2018;51:403–14.
[7] Kovalchenko AM, Goel S, Zakiev IM, Pashchenko EA, Al-Sayegh R. Suppressing scratch-induced brittle fracture in silicon by geometric design modification of the abrasive grits. J Mater Res Technol 2019;8:703–12.
[8] Kumar A, Melkote SN. The chemo-mechanical effect of cutting fluid on material removal in diamond scribing of silicon. Appl Phys Lett 2017;111:011901.
[9] Kayabasi E, Ozturk S, Celik E, Kurt H. Determination of cutting parameters for silicon wafer with a Diamond Wire Saw using an artificial neural network. Sol Energy 2017;149:285–93.
[10] Azar AS, Holme B, Nielsen Ø. Effect of sawing induced micro-crack orientations on fracture properties of silicon wafers. Eng Fract Mech 2016;154:262–71.
[11] Zarudi I, Nguyen T, Zhang LC. Effect of temperature and stress on plastic deformation in monocrystalline silicon induced by scratching. Appl Phys Lett 2005; 86:011922.
[12] Budnitzki M, Kuna M. Scratching of silicon surfaces. Int J Solid Struct 2019;162: 211–6.
[13] Chavoshi SZ, Gallo SC, Dong H, Luo X. High temperature nanoscratching of single crystal silicon under reduced oxygen condition. Mater Sci Eng, A 2017;684: 385–93.
[14] Pala U, Süssmaier S, Kuster F, Wegener K. Experimental investigation of tool wear in electroplated diamond wire sawing of silicon. Procedia CIRP 2018;77:371–4.
[15] Alreja C, Subbiah S. Low pressure phase transformations during high-speed, high-temperature scratching of silicon. ASME J Micro Nano-Manuf. 2018;6:041001.
[16] Zhang Z, Meng F, Cui J, Wang B, Wang Z, Lu Y, et al. Deformation induced complete amorphization at nanoscale in a bulk silicon. AIP Adv 2019;9:025101.
[17] Wu H, Melkote SN. Study of ductile-to-brittle transition in single grit diamond scribing of silicon: application to wire sawing of silicon wafers. ASME J Eng Mater Technol 2012;134(4):041011.
[18] Telyatnik RS. Finite element modeling of nanoindentation and scratching of Si, SiC, Ge crystals with anisotropic plasticity. IOP Conf Ser Mater Sci Eng 2018;387: 012078.
[19] Kumar A, Melkote SN, Kaminski S, Arcona C. Effect of grit shape and crystal structure on damage in diamond wire scribing of silicon. J Am Ceram Soc 2017; 100:1350–9.
[20] Wu H, Melkote SN. Effect of crystallographic orientation on ductile scribing of crystalline silicon: role of phase transformation and slip. Mater Sci Eng, A 2012; 549:200–5.
[21] Yang M, Peng F, Yan R, Deng B, Zhou L, Wang H. Study on the surface damage mechanism of monocrystalline silicon in micro ball-end milling. Precis Eng 2019; 56:223–34.
[22] Gogotsi Y, Zhou G, Ku S-S, Cetinkunt S. Raman microspectroscopy analysis of pressure-induced metallization in scratching of silicon. Semicond Sci Technol 2001;16:345.
[23] Dahmen U, Hetherington CJ, Pirouz P, Westmacott KH. The formation of hexagonal silicon at twin intersections. Scripta Metall 1989;23:269–72.
[24] Kailer A, Gogotsi Y, Nickel K. Phase transformations of silicon caused by contact loading. J Appl Phys 1997;81:3057.
[25] Wang B, Melkote SN, Saraogi S, Wang P. Effect of scratching speed on phase transformations in high-speed scratching of monocrystalline silicon. Mater Sci Eng, A 2020;772:138836.
[26] To S, Wang H, Lee WB. Materials characterisation and mechanism of micro- cutting in ultra-precision diamond turning. Springer-Verlag Berlin Heidelberg; 2018.
[27] Trachet A, Subhash G. Microscopic and spectroscopic investigation of phase evolution within static and dynamic indentations in single-crystal silicon. Mater Sci Eng, A 2016;673:321–31.
[28] Gauthier C, Lafaye S, Schirrer R. Elastic recovery of a scratch in a polymeric surface: experiments and analysis. Tribol Int 2001;34:469–79.
[29] Yang X, Qiu Z, Lu C, Li X, Tang J. Modelling the strain rate sensitivity on the subsurface damages of scratched glass ceramics. Ceram Int 2017;43(15):12930–8.
[30] Rao X, Zhang F, Luo X, Ding F, Cai Y, Sun J, et al. Material removal mode and friction behaviour of RB-SiC ceramics during scratching at elevated temperatures. J Eur Ceram Soc 2019;39(13):3534–45.
[31] Johnson GR, Cook WH. A constitutive model and data for metals subjected to large strains, high strain rates and high temperatures. Hague, Netherlands. In: Proceedings of the seventh international symposium on ballistics; 1983. p. 541–7.
[32] Wang B, Liu ZQ, Song QH, Wan Y, Ren XP. A modified Johnson-Cook constitutive model and its application to high speed machining of 7050-T7451 aluminum alloy. ASME J Manuf Sci Eng 2019;141(1):011012.
[33] Hu JZ, Merkle LD, Menoni CS, Spain IL. Crystal data for high-pressure phases of silicon. Phys Rev B 1986;34:4679.